ACS OMEGA

Article

Cite This: ACS Omega 2019, 4, 2596−2609

http://pubs.acs.org/journal/acsodf

Catalysis of Cu Cluster for NO Reduction by CO: Theoretical Insight into the Reaction Mechanism

Nozomi Takagi,[†] Kazuya Ishimura,[‡] Hiroki Miura,[†,§] Tetsuya Shishido,[†,§] Ryoichi Fukuda,[†] Masahiro Ehara,*[,†,‡] and Shigeyoshi Sakaki*[,†,∥]

[†]Elements Strategy Initiative for Catalysts and Batteries, Kyoto University, 1-30 Goryo-Ohara, Nishikyo-ku, Kyoto 615-8245, Japan

[‡]Institute for Molecular Science, Okazaki 444-8585, Japan

[§]Department of Applied Chemistry, Graduate School of Urban Environmental Sciences, Tokyo Metropolitan University, 1-1, Minami-osawa, Hachioji, Tokyo 192-0397, Japan

[∥]Fukui Institute for Fundamental Chemistry, Kyoto University, 34-4 Takano-Nishihiraki-cho, Sakyo-ku, Kyoto 606-8103, Japan

Supporting Information

ABSTRACT: Density functional theory calculations here elucidated that Cu_{38}-catalyzed NO reduction by CO occurred not through NO dissociative adsorption but through NO dimerization. NO is adsorbed to two Cu atoms in a bridging manner. NO adsorption energy is much larger than that of CO. N−O bond cleavage of the adsorbed NO molecule needs a very large activation energy ($\Delta G^{\circ\ddagger}$). On the other hand, dimerization of two NO molecules occurs on the Cu_{38} surface with small $\Delta G^{\circ\ddagger}$ and very negative Gibbs reaction energy (ΔG°) to form ONNO species adsorbed to Cu_{38}. Then, a CO molecule is adsorbed at the neighboring position to the ONNO species and reacts with the ONNO to induce N−O bond cleavage with small $\Delta G^{\circ\ddagger}$ and very negative ΔG°, leading to the formation of N_2O adsorbed on Cu_{38} and CO_2 molecule in the gas phase. N_2O dissociates from Cu_{38}, and then it is readsorbed to Cu_{38} in the most stable adsorption structure. N−O bond cleavage of N_2O easily occurs with small $\Delta G^{\circ\ddagger}$ and significantly negative ΔG° to form the N_2 molecule and the O atom adsorbed on Cu_{38}. The O atom reacts with the CO molecule to afford CO_2 and regenerate Cu_{38}, which is rate-determining. N_2O species was experimentally observed in Cu/γ-Al_2O_3-catalyzed NO reduction by CO, which is consistent with this reaction mechanism. This mechanism differs from that proposed for the Rh catalyst, which occurs via N−O bond cleavage of the NO molecule. Electronic processes in the NO dimerization and the CO oxidation with the O atom adsorbed to Cu_{38} are discussed in terms of the charge-transfer interaction with Cu_{38} and Frontier orbital energy of Cu_{38}.

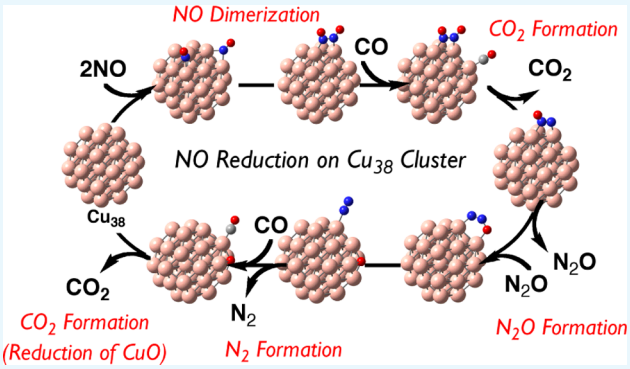

1. INTRODUCTION

The platinum group metals such as platinum, palladium, and rhodium have been exclusively used for three-way catalyst (TWC) for automobiles and electrode catalyst for fuel cells.[1] For cost reduction of catalysts and resource preservation on the earth, the use of abundant metals and/or the reduction of precious metal content in catalysts must be achieved. To design such catalysts, correct understanding of catalytic function of metal cluster/particle is indispensable. However, it is not easy to elucidate experimentally the reaction mechanism and electronic process of a heterogeneous catalytic reaction by metal cluster/particle because experimental tools and analysis techniques are still limited for heterogeneous catalysts even nowadays. In this regard, theoretical investigation of reactivity and catalysis of metal cluster/particle is indispensable.

TWCs catalyze mainly three reactions—oxidation of hydrocarbon to CO_2 and H_2O, oxidation of CO to CO_2, and NO_x reduction to N_2. Among these three reactions, NO reduction by CO has been investigated well both in experiments[2−5] and in theoretical calculations.[6−9] In these studies, the N−O bond cleavage was considered to occur on Rh,[2,3,9] Pt,[6,8] and Pd[5] as one of the key elementary steps.

In recent years, Au nanoscale particles have attracted a lot of interest as new catalysts since the reports by Haruta and co-workers.[10−12] Their reports are of considerable interest because nanoscale Au particles can be applied to catalytic reaction despite the inertness of the bulk metal. Similar catalysts, Au atom (or cluster) doped on M (M = Ni, Rh, Pd, Ag, or Ir), were applied to NO−CO reaction.[13,14] In these studies, the dissociative NO adsorption was proposed as an important initial step like in the NO−CO reaction by Rh, Pt,

Received: October 20, 2018
Accepted: January 10, 2019
Published: February 4, 2019

DOI: 10.1021/acsomega.8b02890
ACS Omega 2019, 4, 2596−2609

Scheme 1. Structure of Cu_{38} and Numbering of Each Atom[a]

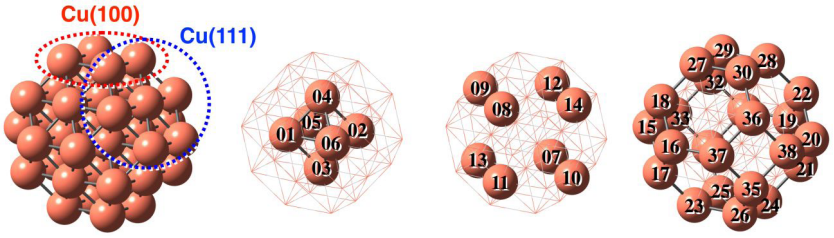

[a]Cu(07) to Cu(14) are center atoms of the (111) plane. Cu(15) to Cu(38) are corner atoms of the (111) plane and belong to the (100) plane at the same time.

Scheme 2. Schematic Representation of the Catalytic Cycle for NO Reduction by CO on Cu_{38}

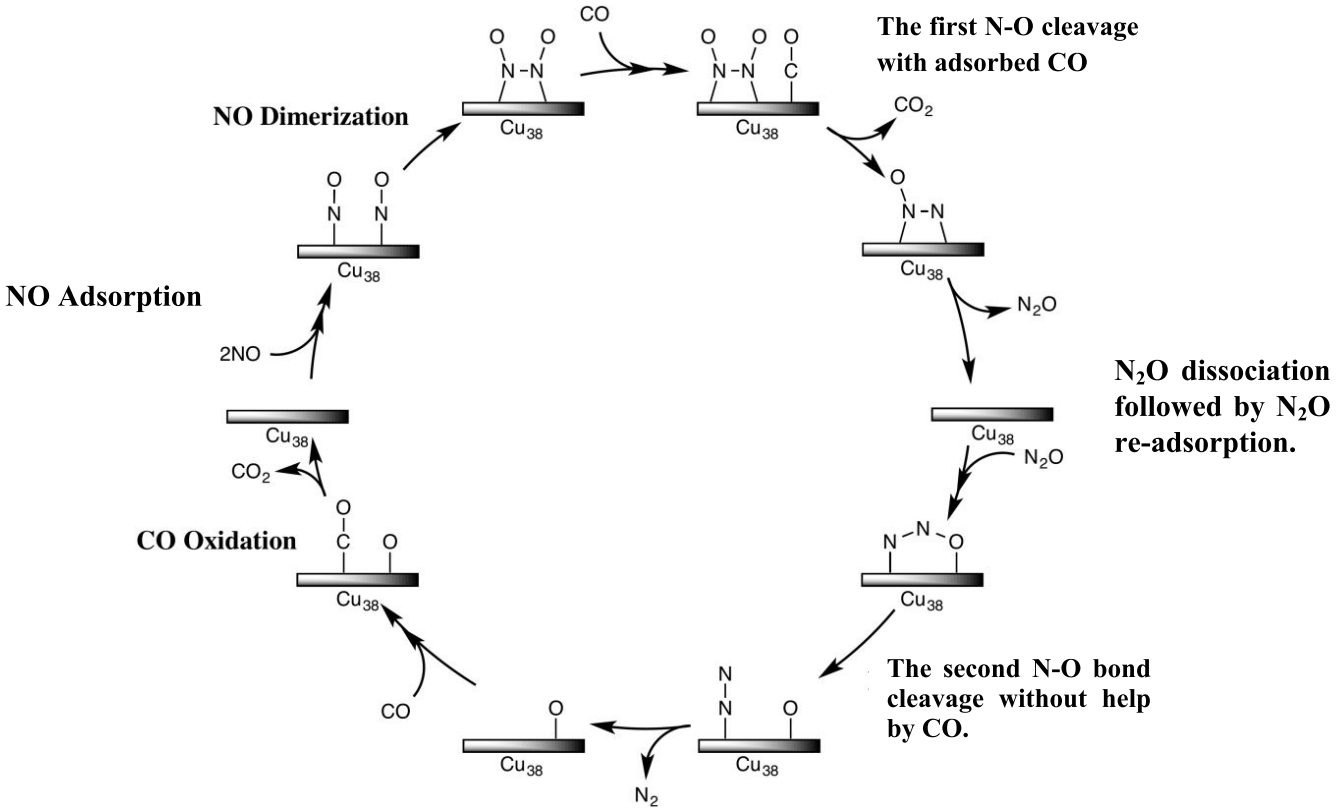

and Pd catalysts.[2,3,5,6,8,9] Also, Ag nanoscale particles were experimentally reported to be active for NO decomposition.[15−18] Pioneering theoretical research reported that the NO decomposition did not occur through dissociative NO adsorption but through NO dimerization.[19−21]

Cu is one of the most abundant metals. Considering catalyses of nanoscale Au and Ag particles and Au-doped metal particles, nanoscale Cu cluster/particle is also expected to be useful as a catalyst. Actually, highly dispersed Cu cluster/particle on γ-Al_2O_3 was reported to exhibit high catalytic activity for NO decomposition and NO reduction by CO.[22−26] Because N−O bond cleavage of the NO molecule is difficult to occur on the Cu surface according to theoretical calculations,[24,27,28] it is likely that NO reduction by this catalyst occurs through a new reaction mechanism without N−O bond cleavage of the NO molecule like the NO reduction catalyzed by Ag nanoclusters.[15−21] It is of considerable interest how and why Cu particles can easily catalyze NO reduction by CO not through N−O bond cleavage of the NO molecule. However, no information has been presented about the reaction mechanism and the full catalytic cycle of Cu-catalyzed NO reduction by CO.

In this work, we investigated the NO reduction by CO on Cu_{38} cluster, using density functional theory (DFT) calculations, where the geometry of Cu_{38} is shown in Scheme 1 with the numbering of each Cu atom. Our purposes here are to elucidate through what reaction mechanism Cu_{38}-catalyzed NO reduction by CO occurs, how easily the N−O bond is cleaved, and what role(s) the Cu cluster plays in this NO reduction by CO. We believe that these computational results are useful for finding a new TWC with nonprecious metals.

DOI: 10.1021/acsomega.8b02890
ACS Omega 2019, 4, 2596−2609

Scheme 3. Possible Reaction Pathways Starting from the NO Adsorption Structure 2b, the NO−CO Coadsorption Structure 4a, and the NO−NO Coadsorption Structure 4b[a]

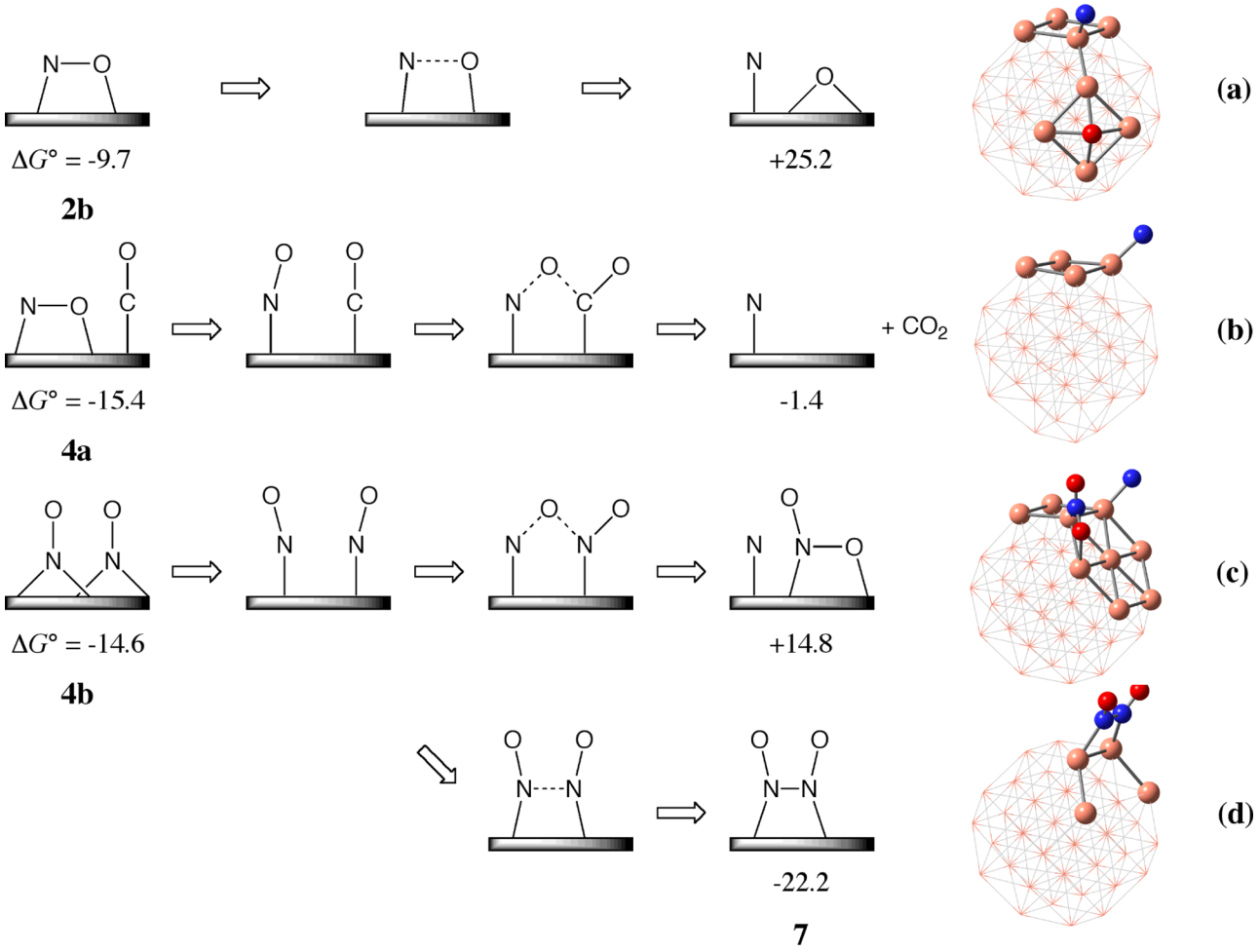

[a]Gibbs energies (ΔG°) relative to the sum of isolated species are presented in kcal/mol.

Scheme 4. Schematic Representation of N−O Bond Cleavage of ONNO Species with and without the Help of CO

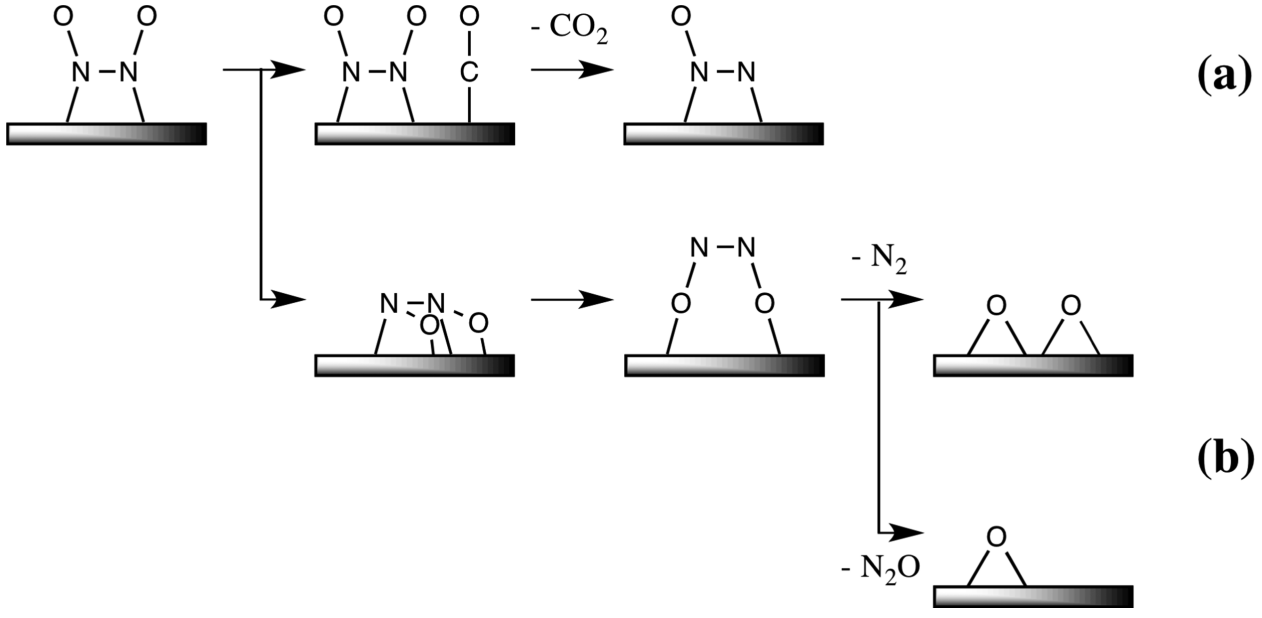

DOI: 10.1021/acsomega.8b02890
ACS Omega 2019, 4, 2596−2609

2. RESULTS AND DISCUSSION

Because many elementary steps will be discussed in this catalytic reaction, we wish to briefly discuss here an overview of the catalytic cycle, as shown in Scheme 2. The first step is NO adsorption to Cu_{38} followed by NO dimerization on the Cu_{38} surface to afford the ONNO dimer. The N−O bond of the ONNO dimer reacts with CO adsorbed on the Cu_{38} to afford CO_2 and N_2O. After readsorption of N_2O to Cu_{38}, the second N−O bond cleavage occurs to afford free N_2 molecule and O atom adsorbed on the Cu_{38} surface. The final step is adsorption of CO followed by the reaction of CO with the O atom on Cu_{38} to afford CO_2 and regenerate the Cu_{38} particle. The rate-determining step is the reaction of CO with the O atom on the Cu_{38} surface. Besides this main reaction course, we investigated other possible reaction courses; for instance, several possible reaction courses of NO including NO dissociative adsorption (Scheme 3) and NO bond cleavage of ONNO species with and without help by the CO molecule (Scheme 4). In the next section, we will discuss each elementary step in detail.

2.1. NO and CO Adsorptions on Cu_{38} Cluster. As the initial step of the NO reduction by CO, we investigated the most favorable adsorption position of the Cu_{38} surface for NO and CO molecules. For NO, we obtained many possible adsorption structures on the Cu_{38} surface such as end-on and side-on with 1-fold, 2-fold, 3-fold, and so on; see Figure S1 in the Supporting Information for all the calculated adsorption structures. Among them, the most stable is the side-on adsorption structure **2b** in which NO is bridging Cu(22) and Cu(28) atoms, as shown in Figure 1, where the spin state is quartet and the Gibbs energy change (ΔG°) for NO adsorption is −9.7 kcal/mol (negative value means stabilization in energy). In **2b**, the NO moiety has negative NBO charge (−0.53e), suggesting that charge transfer (CT) occurs from Cu_{38} to the vacant N−O π^* orbital. The next stable structure is the end-on adsorption structure **2a** in which the N atom is bridging Cu(22) and Cu(28) atoms. Its spin state is a doublet, and its ΔG° is slightly smaller (−9.2 kcal/mol) than that for the side-on adsorption **2b** (Figure 1). The NBO charge (−0.48e) of the NO moiety is also moderately smaller in **2a** than in **2b**, suggesting that the CT from Cu_{38} to the NO moiety is moderately weaker in **2a** than in **2b**.

In CO, only two adsorption structures could be located; both have an end-on adsorption structure through the C atom, as shown in Figure 1. Adsorption structure **3a** at the Cu(30) atom, which is equivalent to Cu(28), is the most stable, where the spin state is a singlet and the ΔG° is moderately negative (−3.9 kcal/mol). This ΔG° is much smaller than that of NO. The CO moiety has positive NBO charge (+0.18e), suggesting that CT occurs from lone-pair orbital of CO to Cu_{38}. Another adsorption structure **3b** was located at the Cu(14) atom, the center of the (111) plane, where the spin state is singlet. However, the ΔG° is positive (+2.1 kcal/mol), indicating that CO is not absorbed at this Cu atom.

On the basis of the above results, it is concluded that NO is more strongly adsorbed on the Cu_{38} surface than CO.

2.2. Dissociative NO Adsorption on Cu_{38} Cluster. In one of the plausible mechanisms, NO reduction by CO with transition-metal catalyst starts to occur by dissociative NO adsorption, as shown in Scheme 3a.[4−9] Because it is likely that N−O bond cleavage starts from the side-on NO adsorbed structure **2b** (Figure 1 and Scheme 3a), we investigated the

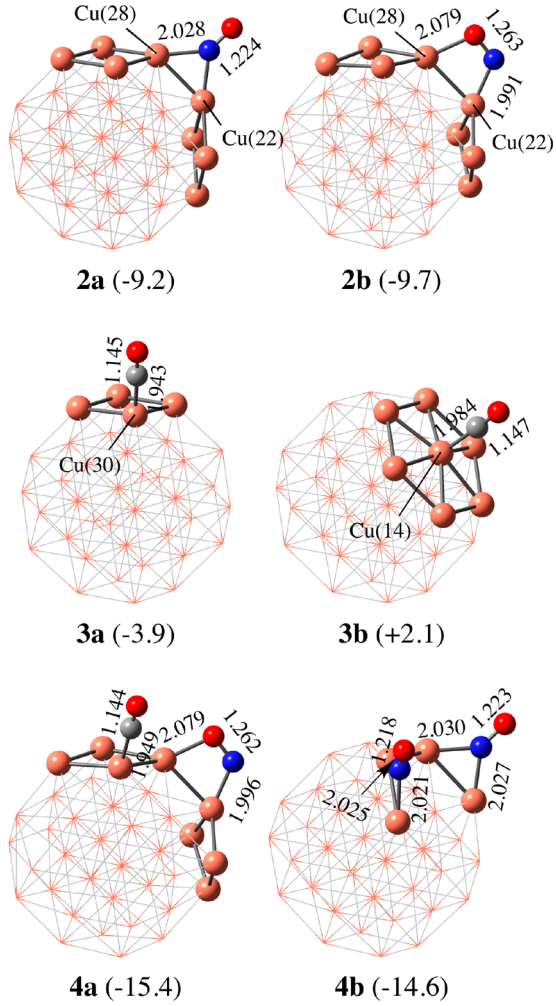

Figure 1. Optimized NO, CO, NO−CO, and NO−NO adsorption structures on Cu_{38}. Distances are in Angstrom. In parentheses are Gibbs energy changes (in kcal/mol) relative to the sum of Cu_{38} and free gas molecule(s).

energy change by elongating the N−O distance in **2b**, where the geometry was optimized at each N−O distance. However, the total energy became significantly higher as the N−O distance was elongated, and the energy barrier was estimated to be very large (more than 80 kcal/mol) for the N−O bond cleavage; the potential energy change is shown in Figure S2a in the Supporting Information. In addition, the product, consisting of N and O atoms separately adsorbed on the Cu_{38} cluster, is much less stable than **2b** by ΔG° = +34.9 kcal/mol. Although this activation barrier for the N−O bond cleavage is smaller than the N−O bond energy of free NO molecules (147.3 kcal/mol), the large ΔG° and large activation barrier clearly show that dissociative NO adsorption on the Cu_{38} surface is energetically difficult to occur, as reported in the previous works.[24,27,28]

It should be concluded that the NO reduction by CO on Cu_{38} occurs without NO dissociative adsorption. We will investigate the below key questions through what elementary step and how the N−O bond cleavage and the N−N bond formation occur in this catalytic reaction.

2.3. N−O Bond Cleavage of NO Molecule by Coadsorbed CO or NO vs N−N Bond Formation between Two NO Molecules. It is likely that the N−O

DOI: 10.1021/acsomega.8b02890
ACS Omega 2019, 4, 2596−2609

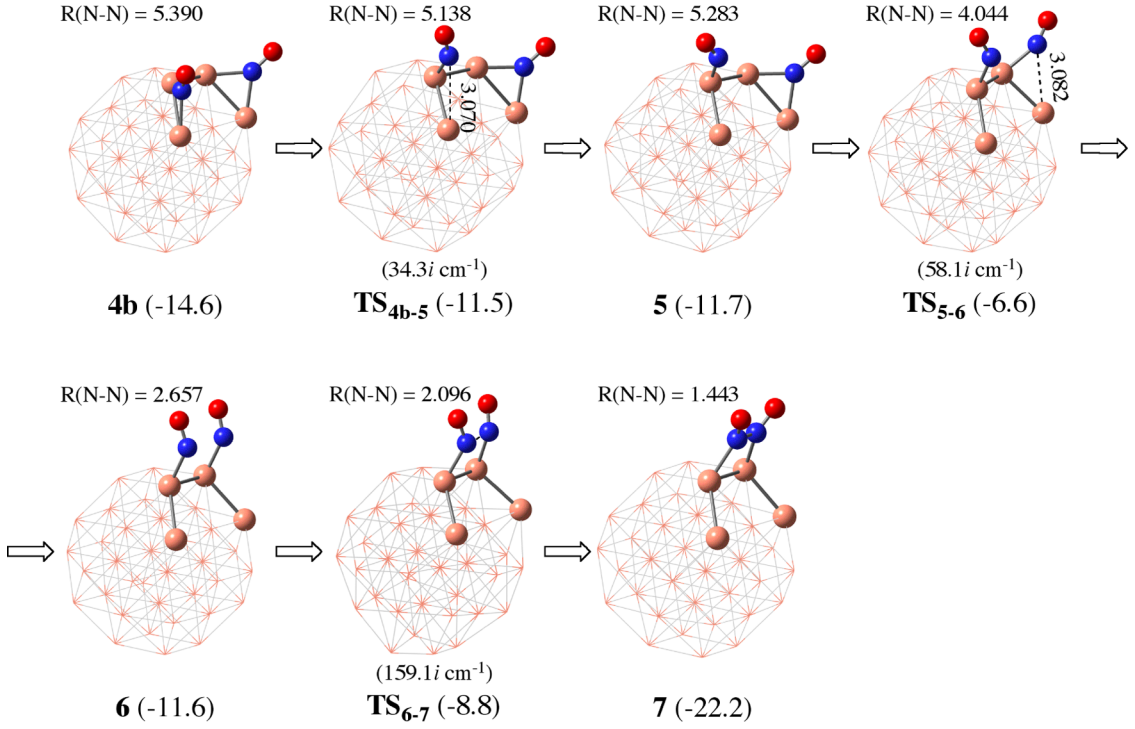

Figure 2. Geometry changes in NO dimerization on Cu_{38}. Distances are in Angstrom. In parentheses are Gibbs energy changes (in kcal/mol) relative to the sum of Cu_{38} and free gas molecule(s).

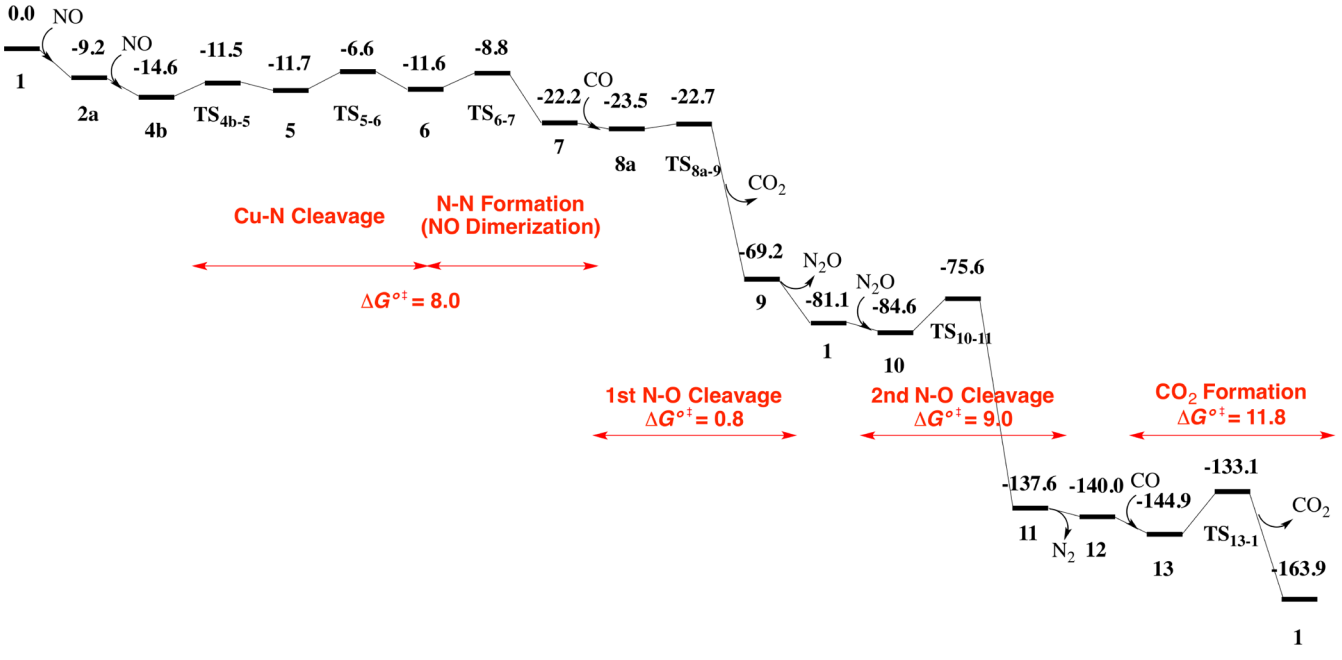

Figure 3. Gibbs energy profile (in kcal/mol) of the NO reduction by CO on Cu_{38} cluster.

bond cleavage occurs by the reaction with CO because thermodynamically stable CO_2 is formed by this reaction (Scheme 3b). The N−O bond cleavage by the reaction with one more NO molecule is also likely to occur, as shown in Scheme 3c, where the NO_2 molecule is produced. Another plausible reaction is NO dimerization affording ONNO species on Cu_{38} because NO dimerization in the gas phase has been well known experimentally[29−31] and proposed in theoretical studies on Co and Au catalysts.[32,33] For the former reaction, NO−CO coadsorption must occur at the neighboring position to each other, and for the latter two reactions, NO−NO coadsorption must occur.

The NO−CO coadsorption structure **4a** was optimized, as shown in Figure 1; the ground state of **4a** has doublet spin multiplicity, but other spin states such as quartet (+0.4 kcal/mol) and sextet (+5.6 kcal/mol) are not very unstable compared to **4a**. Its ΔG° was calculated to be −15.4 kcal/mol relative to the isolated reactants, Cu_{38}, NO, and CO. The coadsorption energy is close to the sum of the separate adsorption energies of NO (ΔG° = −9.7 kcal/mol) and CO

DOI: 10.1021/acsomega.8b02890
ACS Omega 2019, 4, 2596−2609

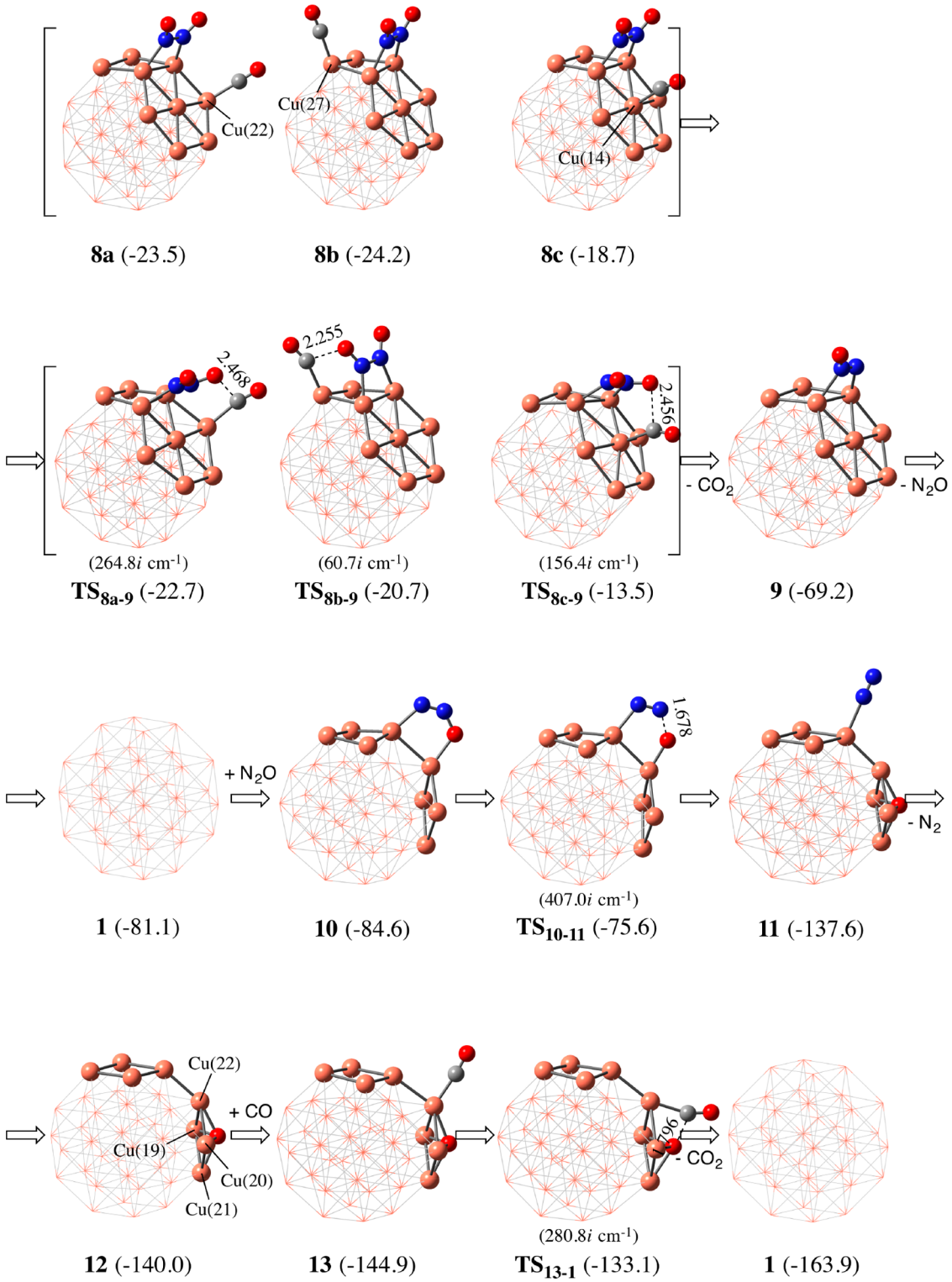

Figure 4. Geometry changes in the reaction of ONNO species with CO on Cu_{38}, affording N_2 and CO_2 molecules. Distances are in Angstrom. In parentheses are Gibbs energy changes (in kcal/mol) relative to the sum of Cu_{38} and free gas molecule(s).

(ΔG° = −3.9 kcal/mol). Another NO−CO coadsorption structure **4c** is somewhat less stable than **4a**, as shown in Figure S1. The N−O bond cleavage by the neighboring CO molecule is endergonic (ΔG° = +14.0 kcal/mol) relative to **4a**. This result suggests that the N atom adsorbed on the Cu_{38} surface is not stable in energy. Thus, this pathway is ruled out hereinafter.

The ΔG° value for NO−NO coadsorption **4b** was calculated to be −14.6 kcal/mol, indicating that this adsorption occurs slightly less favorably than the NO−CO coadsorption, but the energy difference between them is very small (0.8 kcal/mol); the ground state of **4b** has triplet spin multiplicity, but other spin states such as singlet (+2.0 kcal/mol) and quintet (+2.6 kcal/mol) are not very unstable. The second NO molecule is

DOI: 10.1021/acsomega.8b02890
ACS Omega 2019, 4, 2596−2609

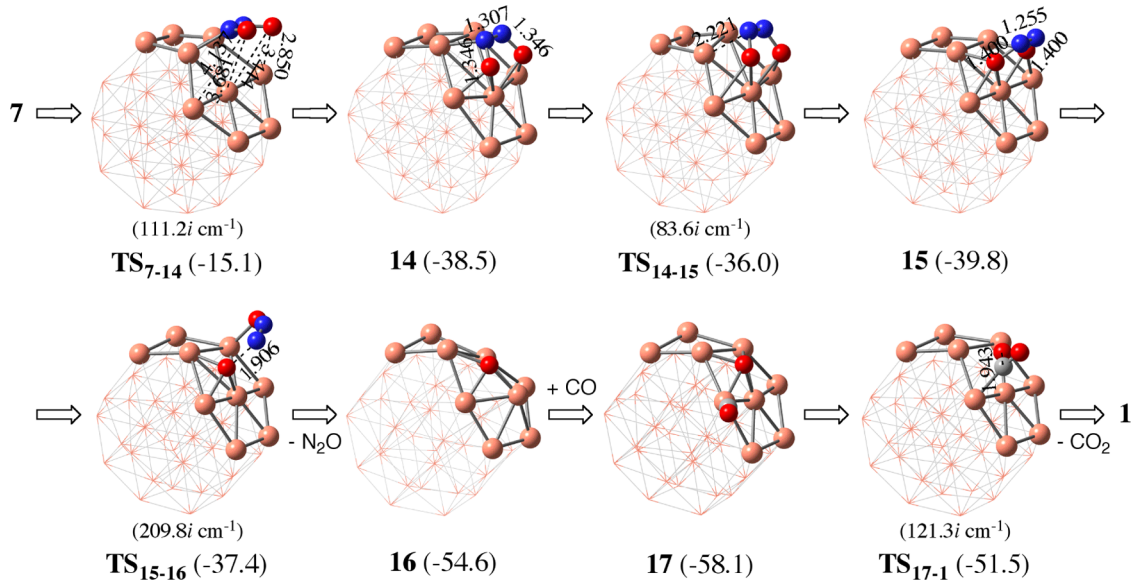

Figure 5. Geometry changes in the NO bond cleavage of the ONNO species on Cu_{38} in the absence of CO, affording N_2O and O atom adsorbed on Cu_{38} (from 7 to **16**) and the reaction of the Cu_{38}-adsorbed O with CO (from **16** to **1**). Distances are in Angstrom. In parentheses are Gibbs energy changes (in kcal/mol) relative to the sum of Cu_{38} and free gas molecule(s).

adsorbed at the neighboring position to the first NO with stabilization energy (ΔG°) of −5.4 kcal/mol, which is smaller than the first one (ΔG° = −9.2 kcal/mol). Other NO−NO coadsorption structures (**4d** and **4e**) are somewhat less stable than **4b**, as shown in Figure S1. Starting from **4b**, N−O bond cleavage assisted by the neighboring NO molecule occurs to afford NO_2 and N atom adsorbed to Cu_{38} with significantly large endergonicity (ΔG° = +29.4 kcal/mol) relative to **4b**, as shown in Scheme 3c, indicating that this pathway is unfavorable. On the other hand, the N−N bond formation via NO dimerization affording ONNO species on the Cu_{38} surface was calculated to be somewhat exergonic (ΔG° = −7.6 kcal/mol) relative to **4b**; see **7** in Scheme 3d.

Because the NO dimerization is much more exergonic than the formations of CO_2 and N atom adsorbed on Cu_{38}, it is likely concluded that the NO dimerization is the most plausible reaction if the $\Delta G^{\circ\ddagger}$ value is not large. Because the N−N distance between two NO molecules is too long (5.390 Å) in **4b** for inducing dimerization reaction between these two NO molecules, we investigated here the reverse reaction starting from **7** to **4b** for convenience and found the geometry changes connecting **4b** and **7**; geometry changes are shown in Figure 2 and the Gibbs energetics is shown in Figure 3. The N−N bond cleavage of the ONNO moiety occurs through transition state $\mathbf{TS_{6-7}}$ to afford intermediate **6**, in which two NO molecules are adsorbed on the Cu_{38} surface in η^1-end-on manner with the N−N distance of 2.657 Å. Starting from **6**, on-top η^1-end-on structure of one NO molecule changes to μ^2-bridging one **5** through transition state $\mathbf{TS_{5-6}}$ (Figure 2). Then, η^1-end-on structure of the other NO molecule changes to μ^2-bridging structure **4b** through transition state $\mathbf{TS_{4b-5}}$. When going from **4b** to $\mathbf{TS_{6-7}}$, the highest energy transition state is $\mathbf{TS_{5-6}}$ and the lowest energy intermediate before $\mathbf{TS_{6-7}}$ is **4b** (Figure 3). Thus, the $\Delta G^{\circ\ddagger}$ going from **4b** to **7** is 8.0 kcal/mol, indicating that the ONNO species is easily formed on the Cu_{38} surface with moderate $\Delta G^{\circ\ddagger}$ and somewhat negative ΔG° value.

The elementary step going from **6** to **7** is crucially important because N−N bond formation occurs in this step. In $\mathbf{TS_{6-7}}$, the N−N distance (2.096 Å) is shorter than in **6** but longer than in **7**. The ONN angles are 112.1 and 112.5°. The geometry of the ONNO moiety in **7** differs very much from the NO dimer experimentally observed in the gas phase.[29] For instance, the N−N distance (1.443 Å) in **7** is considerably shorter than that (2.263 Å) of the free NO dimer. The long N−N distance of the free NO dimer is consistent with the small bond energy (about 2 kcal/mol).[31] Because the NO dimerization process and the ONNO species are crucially important in this reaction, they will be discussed below in a different section.

2.4. N−O Bond Cleavage of ONNO Species. After the formation of the ONNO species on Cu_{38}, two reaction pathways are possible. In one reaction pathway, ONNO reacts with CO, which can be viewed as oxygen atom abstraction by CO, as shown in Scheme 4a. Another is N−O bond cleavage without help by CO (Scheme 4b). In the former pathway, three CO adsorption positions were found neighboring the ONNO moiety on Cu(22), Cu(27), and Cu(14) (**8a**−**8c**), as shown in Figure 4. Among them, the CO adsorption at Cu(27) occurs to afford the most stable coadsorption species **8b**, where the ΔG° is −24.2 kcal/mol relative to Cu_{38}, 2NO, and CO molecules (Figure 3). The next stable CO adsorption occurs at Cu(22) to afford coadsorption structure **8a** (ΔG° = −23.5 kcal/mol), while the difference in ΔG° between **8a** and **8b** is very small (0.7 kcal/mol). The CO adsorption at Cu(14), which is inside the atom of the (111) plane, affords coadsorption structure **8c**, which is considerably less stable (ΔG° = −18.7 kcal/mol) than **8a** and **8b**. Because this CO adsorption is endergonic relative to **7** ($\Delta G_{ads}{}^\circ$ = +3.5 kcal/mol), this coadsorption does not occur and can be ruled out here from the discussion. Starting from **8a**, the N−O bond cleavage occurs much easier via transition state $\mathbf{TS_{8a-9}}$ ($\Delta G^{\circ\ddagger}$ = 0.8 kcal/mol) to afford N_2O-adsorbed Cu_{38} **9** than that starting from **8b**, which occurs via $\mathbf{TS_{8b-9}}$ ($\Delta G^{\circ\ddagger}$ = 3.5 kcal/mol). This small $\Delta G^{\circ\ddagger}$ for $\mathbf{TS_{8a-9}}$ than that for $\mathbf{TS_{8b-9}}$ arises from the much smaller deformation energy (E_{def}) of the Cu_{38}−N_2O moiety in $\mathbf{TS_{8a-9}}$ (E_{def} = 5.0 kcal/mol) than in $\mathbf{TS_{8b-9}}$ (E_{def} = 12.9 kcal/mol), where E_{def} is defined as destabilization

DOI: 10.1021/acsomega.8b02890
ACS Omega 2019, 4, 2596−2609

energy of the Cu_{38}−N_2O moiety when going to $\mathbf{TS_{8-9}}$ from intermediate **8a** or **8b**. It is interesting that the strong N−O bond can be easily cleaved by the CO molecule on the Cu_{38} surface, the details of which will be discussed below.

The N−O bond cleavage without CO participation is also likely to occur because the Cu atom intrinsically wants to bind with the oxygen atom. In this reaction, the ONNO-adsorbed Cu_{38} **7** isomerizes to an isomer **14**, in which the ONNO is parallel to the Cu_{38} surface, as shown in Figure 5. This isomerization occurs through transition state $\mathbf{TS_{7-14}}$ with moderate $\Delta G^{\circ\ddagger}$ of 7.1 kcal/mol and somewhat large ΔG° of −16.3 kcal/mol relative to **7**. Interestingly, **14** further isomerizes to a more stable isomer **15** through transition state $\mathbf{TS_{14-15}}$ with small $\Delta G^{\circ\ddagger}$ (2.5 kcal/mol) and exergonicity (ΔG° = −1.3 kcal/mol) relative to **14**. In **15**, two oxygen atoms of the ONNO moiety interact with Cu_{38}. Although flipping of the ONNO moiety on the same Cu atoms is another plausible isomerization course of **7** to **15**, an intermediate for the flipping isomerization, in which the ONNO moiety is almost perpendicular to the (111) facet (**24** in Figure S3), was calculated to be more unstable than **7** by 9.1 kcal/mol. This energy is larger than the $\Delta G^{\circ\ddagger}$ value for $\mathbf{TS_{7-14}}$ (7.1 kcal/mol), indicating that the flipping isomerization is not easy to occur. Starting from **15**, the N−O bond cleavage occurs through transition state $\mathbf{TS_{15-16}}$ with a small activation energy ($\Delta G^{\circ\ddagger}$ = 2.4 kcal/mol) to afford **16** and a free N_2O molecules with significant exergonicity (ΔG° = −14.8 kcal/mol) relative to **15**. These results indicate that the N−O bond cleavage of the ONNO species easily occurs on the Cu_{38} surface even in the absence of CO. This reaction corresponds to NO decomposition without CO because N_2O is easily converted to N_2 molecule and O atom adsorbed to Cu_{38}, as will be discussed below. However, this NO decomposition occurs less easily than the NO reduction by CO because the isomerization of **7** to **14** needs much larger $\Delta G^{\circ\ddagger}$ (7.1 kcal/mol) than that (0.8 kcal/mol) of the reaction of **7** with CO via $\mathbf{TS_{8a-9}}$.

In the other reaction starting from **15**, two N−O bonds are simultaneously cleaved through the concerted transition state $\mathbf{TS_{15-18}}$ to afford an N_2 molecule in one step, as shown in Figure S4 in the Supporting Information. The $\Delta G^{\circ\ddagger}$ value (10.7 kcal/mol) is larger than that of the above-mentioned pathway, indicating that simultaneous cleavage of two N−O bonds is difficult to occur. In addition, we investigated the formation of anionic $[ONNO]^-$ species from **7**, considering the previous report of its formation,[34] but found that it was highly endergonic by 118 kcal/mol, indicating that such process is difficult to occur.

In summary, the N−O bond cleavage of the ONNO species occurs through reaction with CO adsorbed at the neighboring site of the ONNO species to afford N_2O and CO_2. In the absence of CO, the N−O bond cleavage of ONNO occurs after the isomerization **7** → **14** → **15** to afford N_2O and O atom adsorbed to Cu_{38}, but it needs larger $\Delta G^{\circ\ddagger}$ value than the N−O bond cleavage of ONNO by CO.

2.5. N_2 Formation from N_2O through N−O Bond Cleavage. We investigated here if the N−O bond cleavage of N_2O occurs through reaction with the CO molecule starting from **9** (N_2O-adsorbed Cu_{38}). Three possible CO adsorption positions were found neighboring the N_2O moiety adsorbed on Cu(36), Cu(27), and Cu(14) (**19a**−**c** in Figure S5). Although the CO adsorption (**19c**) occurs at Cu(14) with moderate endergonicity relative to **9** (ΔG_{ads}° = +0.7 kcal/mol), the other CO adsorption (**19a** and **19b**) occurs at Cu(36) and Cu(27) atoms with somewhat large exergonicity (ΔG_{ads}° = −8.0 and −6.0 kcal/mol, respectively). However, N_2O dissociation from the Cu_{38} surface into the gas phase occurs more easily than these CO adsorptions because the ΔG° value is much more negative (−11.9 kcal/mol) relative to **9** than the CO adsorption. This means that N_2O can be observed as an intermediate in the gas phase, which will be discussed below based on the experimental finding. Subsequently, N_2O readsorption easily occurs to produce the most stable N_2O adsorption structure **10**, where the ΔG° is −15.4 kcal/mol relative to **9**.

Starting from **10**, the second N−O bond cleavage occurs through transition state $\mathbf{TS_{10-11}}$ to afford an N_2 molecule and O atom adsorbed to Cu_{38} **11**, as shown in Figure 4. The $\Delta G^{\circ\ddagger}$ value (9.0 kcal/mol) is larger than that of the first N−O bond cleavage, although the exergonicity is significantly large (ΔG° = −53.0 kcal/mol) relative to **10**, as shown in Figure 3. The N_2 molecule dissociates from Cu_{38} with ΔG° = −2.4 kcal/mol relative to **11** to afford an intermediate **12**, in which the O atom is bound at the hollow site of Cu(19), Cu(20), Cu(21), and Cu(22) atoms; see Figure 4. The CO molecule is adsorbed at one of these four Cu atoms neighboring the O atom with ΔG_{ads}° of −4.9 kcal/mol, which is moderately larger than that of **1** (ΔG_{ads}° = −3.9 kcal/mol). This is reasonable because the surface Cu atoms become electron deficient by the adsorbed O atom to enhance σ donation from the CO lone pair to Cu_{38}; as mentioned above, CO interacts with Cu_{38} by the σ donation. The CO molecule reacts with the O atom through transition state $\mathbf{TS_{13-1}}$ to produce CO_2 and regenerate Cu_{38} with $\Delta G^{\circ\ddagger}$ of 11.8 kcal/mol (Figure 3).

As another possibility, we investigated N−O bond cleavage of N_2O assisted by the CO molecule in **10**. However, CO is adsorbed at the Cu atom neighboring the N_2O to afford intermediate **20** with ΔG° = −5.9 kcal/mol relative to **10**, as shown in Figure S6 in the Supporting Information. We tried to find a concerted reaction course via simultaneous N−O and Cu−O bond cleavages with CO_2 formation, but could not. Instead, the N−O bond cleavage occurs without any interaction with CO at the neighboring site (Figure S6) to afford an N_2 molecule and **13**. This process occurs with $\Delta G^{\circ\ddagger}$ value of about 10 kcal/mol, which is moderately larger than that for $\mathbf{TS_{10-11}}$ ($\Delta G^{\circ\ddagger}$ = 9.0 kcal/mol). Thus, it should be concluded that the second N−O bond cleavage occurs easier without CO coordination than that by CO molecule. This is true because the adsorbed CO molecule increases the electron population of the Cu surface to enhance the bonding interaction between the O atom and the Cu_{38} surface.

The smaller adsorption energy of CO (**13**) than the activation energy for CO_2 formation ($\mathbf{TS_{13-1}}$) may induce oxygen accumulation on the Cu surface. To explore this possibility, we calculated the CO_2 formation process from Cu_{38} with two O atoms **21**, as shown in Figure S7. The ΔG° for CO adsorption to **21** is −12.5 kcal/mol, which is much larger than that to **12** with one O atom (−4.9 kcal/mol), suggesting that CO adsorption energy increases as the number of O atoms increases on the Cu surface; this is not surprising because the O atom is electron-withdrawing from Cu_{38} to enhance CT from CO to Cu_{38}. The $\Delta G^{\circ\ddagger}$ for CO_2 formation is calculated to be 9.4 kcal/mol, which is somewhat smaller than that from **12** with one O atom (11.8 kcal/mol). In addition, ΔG° for CO_2 formation is −37.5 kcal/mol, which is considerably larger than the ΔG° for CO_2 formation from **12** (−23.9 kcal/mol).

DOI: 10.1021/acsomega.8b02890
ACS Omega 2019, 4, 2596−2609

These results suggest that the presence of many O atoms on the Cu surface enhances CO adsorption, decreases the $\Delta G^{\circ\ddagger}$ value, and increases exergonicity for CO_2 formation and that oxygen accumulation does not occur on the Cu surface. Actually, the X-ray diffraction (XRD) and X-ray photoelectron spectroscopy of the Cu/Al_2O_3 catalyst produced with 5 vol% H_2/He at 773 K showed that copper oxides (CuO and Cu_2O) were not detected.

Instead of CO adsorption, NO reaction with **12** affording NO_2 is another possible reaction. The calculations show that the NO molecule can be adsorbed on **12** in the bridging form (**23a** and **23b**) neighboring the O atom (see Figure S8), whereas the on-top NO adsorption structure could not be located. The ΔG° values for NO adsorption are −10.5 (**23a**) and +0.4 (**23b**) kcal/mol, indicating that NO can be adsorbed to form intermediate **23a**. However, the ΔG° for NO_2 formation is much endergonic relative to **23a** (+39.0 kcal/mol), suggesting that $\Delta G^{\circ\ddagger}$ for NO_2 formation must be larger than it. As discussed above, on the other hand, the CO_2 formation is highly exergonic. Based on these results, it is likely concluded that NO_2 formation is energetically difficult but CO_2 formation can occur.

The Gibbs energetics for the best reaction pathway is summarized in Figure 3, which shows that this catalytic reaction is apparently downhill with moderate $\Delta G^{\circ\ddagger}$ and significantly large exergonicity (significantly negative ΔG°). The rate-determining step is the CO_2 formation reaction between CO and the O atom adsorbed to Cu_{38} ($\Delta G^{\circ\ddagger}$ = 11.8 kcal/mol), which corresponds to the reduction of $Cu_{38}O$ with CO. This is reasonable because Cu has strong affinity to oxygen.

2.6. Details of Electronic Process in the Formation of ONNO Species on Cu_{38} and Oxidation of CO with O Atom Adsorbed on Cu_{38}. In this section, a discussion is presented on electronic processes of NO dimerization on the Cu_{38} surface and CO oxidation with the O atom adsorbed on Cu_{38} because CO oxidation is the rate-determining step and NO dimerization is a key step for NO reduction by CO on the Cu_{38} surface.

As discussed above, the short N−N distance (1.443 Å) and the large N−N bond energy (10.6 kcal/mol; evaluated by ΔG°(**7**−**6**)) of the ONNO species on Cu_{38} significantly differ from those of the NO dimer in the gas phase (2.263 Å and 2 kcal/mol, respectively).[29−31] Previous theoretical works of the NO dimer[35−38] in the gas phase reported that the electronic structure of the NO dimer has a multireference character because of the presence of nearly degenerated π and π^* orbitals of two N−O bonds. This means that the DFT method cannot be applied to the NO dimer. Here, we investigated the NO dimer (ONNO species) on the Cu_2 model system using the complete active space self-consistent field (CASSCF) method and found that the electronic structure of the NO dimer on the Cu_2 cluster can be described well by the DFT method; details are presented in Pages S10−S13 in the Supporting Information. This result suggests that the DFT method can be applied to the NO dimerization on the Cu cluster/particle.

The intermediate $Cu_{38}(NO)_2$ **6** has two NO molecules adsorbed to Cu_{38} (Figure 2), in which CT occurs from Cu_{38} to two NO molecules by about 0.4*e*, as shown in a solid green line in Figure 6. Interestingly, the CT becomes stronger, on going to $\mathbf{TS}_{6-7}$ (0.46*e*) and **7** (0.50*e*) from **6**. The difference in NBO charge between free ONNO and adsorbed ONNO to Cu_{38}

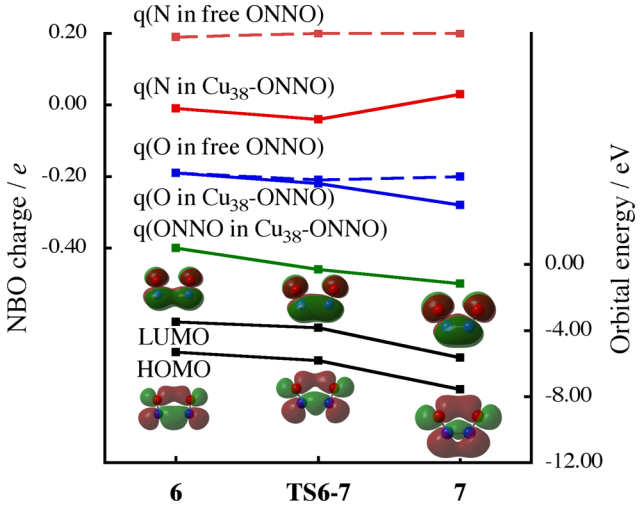

Figure 6. Changes of NBO charges of the ONNO moiety of Cu_{38}-ONNO on going from **6** (two NO molecules) to **7** (ONNO species) through $\mathbf{TS}_{6-7}$ (solid line) in comparison with those of free ONNO molecules (dashed line).[a] Frontier orbital energies and their figures are drawn for free ONNO molecules. NBO charge and orbital energy are in *e* and eV, respectively. [a]The geometry of free ONNO molecules is taken from **6**, $\mathbf{TS}_{6-7}$, and **7**.

(between the solid and dashed lines) shows that the CT significantly occurs to the N atoms, where the geometry of free ONNO was taken to be the same as that of the ONNO adsorbed to Cu_{38} for comparison. The lowest unoccupied molecular orbital (LUMO) of free ONNO species consists of bonding overlap between π^* orbitals of the NO bond; see the LUMO figure shown in Figure 6. On going from **6** to **7**, the LUMO energy of the free ONNO species becomes significantly lower because the N−N distance becomes shorter (Figure 6). As a result, the CT from Cu_{38} to ONNO becomes stronger and simultaneously enhances the N−N bonding interaction. Also, the CT contributes to the N−O bond weakening because the LUMO is antibonding between N and O atoms. Because of this CT, the N−O bond is easily cleaved after the formation of ONNO on Cu_{38}. Consistent with this CT, the highest energy occupied MO (φ_{HO}) localized on the Cu_{38} surface, which plays an important role in charge transfer to NO molecules from Cu_{38}, becomes lower in energy on going to **7** (−6.36 eV) from **6** (−5.96 eV); see Figure S10 in the Supporting Information. This result suggests that the metal particle bearing φ_{HO} at high energy is favorable for NO dimerization, as was discussed recently.[39] For instance, the NO dimerization occurs on Cu_5 with the activation energy of 9.4 kcal/mol,[39] which is much larger than that (2.8 kcal/mol) on the Cu_{38}. This significant difference between Cu_5 and Cu_{38} can be explained in terms of the lower φ_{HO} energy of Cu_5 (−5.58 eV) than that of Cu_{38} (−4.29 eV).

In the CO reaction with the O atom adsorbed on Cu_{38}, the sum of electron populations of CO and O becomes moderately more negative at $\mathbf{TS}_{13-1}$ but then changes to zero in CO_2 at **1** + CO_2. Though the electron population of Cu_{38} moderately decreases at $\mathbf{TS}_{13-1}$, it finally increases at **1** + CO_2; see Table S1 in the Supporting Information. This population change is consistent with our understanding that the conversion of Cu_{38}−O **13** to Cu_{38} is a two-electron reduction reaction. Consistent with this understanding, the lowest energy unoccupied MO φ_{LU} of **13** becomes the highest energy occupied MO φ_{HO} in **1**; see Figure S11. Thus, the M_n−O (M

DOI: 10.1021/acsomega.8b02890
ACS Omega 2019, 4, 2596−2609

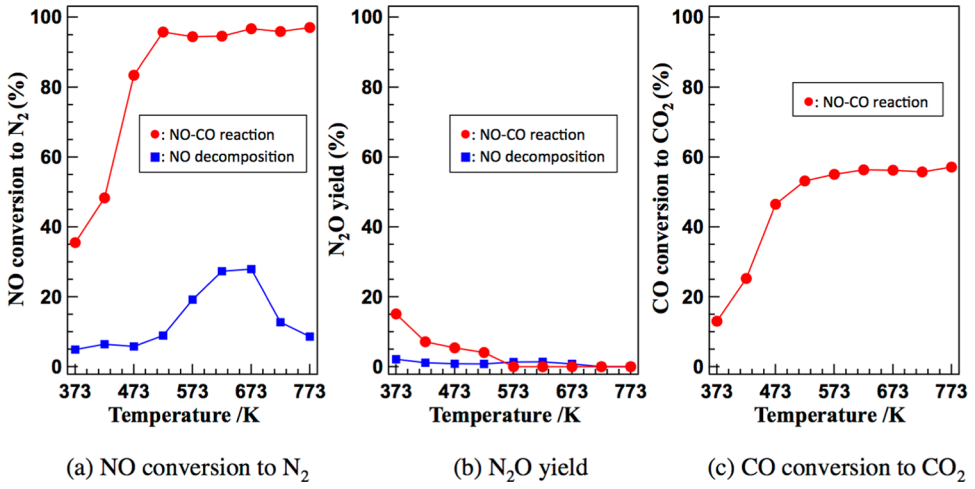

Figure 7. Experimental results for (a) NO conversion to N_2 (%), (b) N_2O yield (%), and (c) CO conversion to CO_2 (%) in NO−CO and NO decomposition reactions in the Cu/γ-Al_2O_3 catalyst.[a] [a]The reaction time was 1 h at every temperature. The reaction temperature was increased from 373 to 573 K in a step-by-step manner. The temperature was kept constant for 1 h at every temperature. We recorded the activity (NO conversion to N_2) every 15 min, and the activity was stable for 1 h.

= metal) species bearing φ_{LU} at low energy is favorable for the CO oxidation step.

In summary, the electronic structure of the ONNO moiety on Cu_{38} is quite different from that of the free NO dimer in the gas phase. Significant CT occurs from the Cu_{38} to the ONNO species, which contributes to the stability of the ONNO species with a short N−N bond, the large N−N bond energy, and simultaneously the weakening of the N−O bond. In the CO oxidation step, the sum of electron populations of CO and O atom decreases. It is likely concluded that the metal particle M_n bearing φ_{HO} at high energy is favorable for NO dimerization and the M_n−O species bearing φ_{LU} at low energy is favorable for CO oxidation.

2.7. Relation to Experimental Findings. If the above reaction mechanism is correct, N_2O species must be detected in the experiment. We carried out an experiment of NO reduction by CO using Cu nanoparticles supported by γ-Al_2O_3. Figure 7 shows the results of the reaction and NO decomposition over the 5 wt % Cu/γ-Al_2O_3 catalyst at 373−773 K. In the case of NO−CO reaction, NO was reduced to N_2 even at low temperature (373 K), and a small amount of N_2O was detected. The formation rate of N_2 increased as the reaction temperature increased. On the contrary, N_2O yield decreased as the reaction temperature increased, suggesting that the rate-determining step occurs after N_2O formation. In our calculation, the rate-determining step is CO oxidation by O atom adsorbed on Cu_{38}, which exists after N_2O formation.

A quite weak diffraction peak due to Cu(111) was detected around 43.4° in the XRD pattern of 5 wt % Cu/γ-Al_2O_3 reduced at 773 K with 5 vol % H_2/He (Figure S12 in the Supporting Information). This result indicates that Cu metal nanoparticles were highly dispersed on the γ-Al_2O_3 surface. The XRD pattern showed a very weak and broad diffraction peak around 2θ = 43−44°, which corresponds to the peak by the Cu particle, indicating that the diameter of the Cu cluster is less than 2 nm (Figure S12). Though the size of the Cu particle employed in the experiment is not very large, it is likely that the real Cu particle used in the experiment is larger than the Cu_{38} employed for the calculations here, suggesting that further work is needed for investigating size effects on the NO−CO reaction by the Cu particle. The γ-Al_2O_3 without Cu exhibited a quite low activity (no data shown here), indicating that Cu loading was indispensable for NO reduction activity. Thus, it is likely concluded that the NO reduction by CO takes place on highly dispersed Cu metal nanoparticles. However, this result does not mean that the interface between the Cu metal nanoparticle and the Al_2O_3 surface does not participate in the reaction. Such NO−CO reaction on the interface was not investigated in this work, and thereby the reaction on the interface should be theoretically investigated in future because such an interface effect is important in catalysis.

The direct NO decomposition also occurred by 5 wt % Cu/γ-Al_2O_3, and the formation rate of N_2 was increased as the reaction temperature increased up to 673 K, but then decreased. A small amount of N_2O was detected together with N_2. These results are also consistent with the computational result that NO decomposition can occur even in the absence of CO.

3. CONCLUSIONS

NO reduction by CO on an octahedral Cu_{38} cluster was theoretically investigated with the DFT method. NO is adsorbed to Cu_{38} in the bridging form between two Cu atoms. The side-on adsorption structure is slightly more stable than the end-on structure. In the case of CO, only the on-top end-on adsorption structure is located. The NO adsorption energy is somewhat larger than that of CO adsorption. Though dissociative NO adsorption is often discussed to occur in many TWCs, the present DFT calculation clearly shows that dissociative NO adsorption on Cu_{38} needs significantly large activation energy and endergonicity, suggesting such adsorption is difficult.

Then, we investigated the NO reduction by CO starting from NO−CO and NO−NO coadsorption structures on Cu_{38}. Starting from the NO−CO coadsorption structure, N−O bond cleavage occurs through O abstraction by CO to afford CO_2, and the N atom adsorbed to Cu_{38}. However, this is significantly endergonic, suggesting that this is difficult to occur. Starting from the NO−NO coadsorption structure, the N−O bond cleavage occurs through O abstraction by another NO but it is significantly endergonic. Starting from the NO−NO coadsorption structure, on the other hand, NO

DOI: 10.1021/acsomega.8b02890
ACS Omega 2019, 4, 2596−2609

dimerization occurs with a very small activation energy and significant exergonicity to produce ONNO species on Cu_{38}. On the basis of these results, it is reasonably concluded that the N−N bond formation occurs through NO dimerization as the initial step of this catalytic NO reduction by CO.

Notably, the ONNO species on the Cu_{38} cluster has a significantly shorter N−N distance than that of the free ONNO species in the gas phase, which has a much longer and weaker N−N bond. The analysis of the electronic structure shows that CT significantly occurs from Cu_{38} to the N−N bonding orbital of the ONNO species to stabilize this ONNO species. The electronic structure of the ONNO moiety on Cu_{38} differs very much from that of the free NO dimer in the gas phase.

After the formation of the ONNO species on Cu_{38}, the N−O bond cleavage easily occurs through O abstraction by the coadsorbed CO molecule at the neighboring position to produce N_2O-adsorbed Cu_{38} and free CO_2 molecule. It should be noted that a strong N−O bond can be easily cleaved on the Cu surface by CT from Cu_{38} to the ONNO species because the CT leads to weakening of the N−O bond. N_2O dissociates from Cu_{38} into the gas phase with somewhat large exergonicity, and then it is adsorbed to Cu_{38} again in the most stable adsorption structure with moderate exergonicity. After readsorption of N_2O to Cu_{38}, the second N−O bond cleavage occurs to afford N_2- and O-adsorbed Cu_{38} with small activation energy and significant exergonicity. The thus-formed N_2 molecule easily dissociates from Cu_{38}, and the remaining O atom on Cu_{38} reacts with the adsorbed CO molecule to produce CO_2 molecule and regenerate Cu_{38}; thus, the catalytic cycle is completed. The rate-determining step is the final CO_2 formation because the Cu cluster has large oxygen affinity.

The formation of N_2O and its dissociation from Cu_{38} into the gas phase are consistent with the experimental finding that N_2O is observed in Cu/γ-Al_2O_3-catalyzed NO reduction by CO.

The reaction mechanism here completely differs from that for the Rh particle in which NO dissociative adsorption occurs as an important elementary step. This result here strongly suggests that a nonprecious metal such as Cu can be applied to the automotive deNO_x catalyst through a new reaction mechanism. The role of Cu_{38} in this catalytic reaction is attributed to CTs from Cu_{38} to ONNO species, which is crucially important for formation of ONNO species and N−O bond cleavage of the ONNO species. At the end of this section, we wish to mention that Cu_{38} is not general but smaller than a real catalyst, as will be described in the section of models. Thus, size effects of Cu particles on NO−CO reaction must be investigated in the near future; see Figure S2b,c for preliminary computational results showing moderate size effects on NO dimerization by the Cu nanocluster.

4. COMPUTATIONAL DETAILS AND MODELS

All geometries were optimized by the DFT method with the hybrid B3LYP functional.[40−42] Though it is said that metal properties cannot be represented well by the hybrid functional,[43] we employed the B3LYP functional because the B3LYP computation provided similar results of geometry and spin state to those by various functionals including typical generalised gradient approximation-type functionals[44] after comparison with Perdew−Burke−Ernzerhof-calculated results; see Table S2 and the brief discussion below it. For the Cu atom, the LANL2DZ[45] basis set was employed, where the core electrons were replaced with the effective core potentials. Because the LANL2DZ is not very large and prone to basis set superposition error (BSSE), we made the BSSE correction for typical CO and NO adsorbed structures on Cu_{38} using the counterpoise procedure shown in Table S3 and the explanation below it. However, the discussion and conclusion do not change by using these results with the BSSE correction. For C, N, and O atoms, Huzinaga−Dunning's split-valence basis sets[46] were employed, where one *d* polarization function was added. We checked in our previous work that the B3LYP/LANL2DZ calculation presented essentially the same geometry and relative energy to coupled cluster single and double substitutions with perturbative triples (CCSD(T)) calculation with triple-ζ basis sets for such diatomic systems as Cu−Cu, Cu−M, and M−M (M = Ru, Rh, Pd, Ag, Os, Ir, Pt, and Au). Also, this method was successfully applied to the geometry and electronic structure of Cu_{38} and $M_6@Cu_{32}$ core−shell cluster with the M_6 core (M = Ru, Rh, Pd, Ag, Os, Ir, Pt, and Au).[44] The CASSCF[47] method was used for NO dimerization on Cu_2 using cc-pVTZ basis sets.[48] In the CASSCF calculations, 16 electrons in 14 orbitals were taken as the active space, where 2 π (in-plane and out-of-plane) and 2 π^* MOs (in-plane and out-of-plane) between N and O atoms, σ-bonding and σ^*-antibonding MOs between N and O atoms, and 4s−4s bonding and antibonding MOs between Cu atoms were included in the active space. Though the convergence test of the active space size was not performed in this work, the CASSCF(16, 14) presents similar energy changes to CCSD(T) calculation.[39]

The Gaussian09[49] and SMASH[50] programs were used for the DFT calculations, and the GAMESS[51] program was used for the CASSCF calculations.

Octahedral-like Cu_{38} cluster **1** was chosen here as a model of the Cu nanocluster because the octahedral-like Cu_{38} was previously reported as the most stable structure of Cu_{38}, which possesses Cu(111) planes of the face-centered cubic structure;[52] the Cu(100) plane is found in Cu_{38}, but all Cu atoms of the (100) plane are vertices, suggesting that its properties differ from those of Cu atoms of the usual (100) plane. Because the NO dimer was experimentally observed on Cu(100) and Cu(111) surfaces,[53−57] **1** was employed as a model of the Cu nanocluster catalyst for NO−CO reaction. In Cu_{38}, 6 Cu atoms form an octahedral Cu_6 core, and 32 Cu atoms form the surface of Cu_{38}, as shown in Scheme 1. In the surface, 8 Cu atoms take center position of the (111) plane, whereas the other 24 Cu atoms belong to the (100) plane and at the same time the (111) plane. Though the XRD pattern measured in this work indicated that the size of the Cu particle was smaller than 2 nm, as was discussed above, it is likely that the real Cu particle is larger than Cu_{38}. We wish to summarize the weak points of this model below. The calculation showed that the adsorption of NO occurs at the Cu(22) and Cu(28) atoms on the adjacent (100) planes, but such adjacent (100) planes disappear for larger Cu particles. Thus, Cu_{38} particles may not be in the scalable regime of realistic clusters, which is one weak point of this model. Therefore, further theoretical work must be performed on the size effect of metal cluster on NO−CO reaction in the future. In such future works, computational results on Cu_{38} would be valuable because comparison between Cu_{38} and other sizes can be made. Also, we wish to mention here that Al_2O_3 support was not involved in this modeling though the reaction was experimentally carried out on the Al_2O_3 support. In the presence of the Al_2O_3

DOI: 10.1021/acsomega.8b02890
ACS Omega 2019, 4, 2596−2609

support, charge transfer (CT) occurs between Al_2O_3 and Cu_{38},[20,21,58] and the geometry deformation of Cu_{38} would be induced by the interaction with Al_2O_3. Besides them, we must remember that the interface between Cu_{38} and Al_2O_3 participates in the catalytic reaction. These effects could not be involved in the calculation of this work due to the heavy cost of such calculations; these important issues must be theoretically investigated in the future.

The ground state of Cu_{38} has triplet spin multiplicity.[44] The spin multiplicities and the S^2 eigenvalues for the calculated species are summarized in Table S4. The results show that the spin contamination is small for all the species.

The energetics of the reaction is discussed with the Gibbs energy. In Cu_{38}, translational and rotational movements were not taken into account for entropy and thermal correction terms but only vibrational movements were taken because the Cu_{38} cluster is not a gas molecule. In free NO, CO, N_2O, N_2, and CO_2 molecules, the usual entropy term and thermal correction by translational, rotational, and vibrational movements were employed for the Gibbs energy. All geometries were optimized without any constraint.

5. EXPERIMENTAL DETAILS

γ-Al_2O_3 (JRC-ALO-7) was provided by the Catalysis Society of Japan. First, 5 wt % Cu/γ-Al_2O_3 was prepared by the impregnation method. Cu aqueous solution was prepared by dissolving $Cu(NO_3)_2{\cdot}3H_2O$. The support was added to the mixture of deionized water and the Cu solution, followed by evaporation. It was dried at 353 K. The resulting powder was calcined in air at 773 K for 5 h.

The NO−CO reaction was carried out in a fixed-bed flow reactor at atmospheric pressure. The Cu/γ-Al_2O_3 catalyst (5 wt %; 200 mg) was placed in a tubular reactor. The reaction gas (100 mL/min), consisting of 1000 ppm NO, 1000 ppm CO, and He as the balance, was introduced to the catalyst bed. Before the reaction, the catalyst was heated to 773 K in a stream of 5 vol % H_2/He for 1 h. The effluent gases from the reactor were analyzed by gas chromatography (Shimadzu GC-8A, Porapak Q and MS-5A columns) equipped with a thermal conductivity detector.

Catalytic NO decomposition experiment was also performed in a fixed-bed reactor as described above. The reaction gas (100 mL/min), consisting of 1000 ppm NO and He as the balance, was introduced to the catalyst (200 mg).

■ ASSOCIATED CONTENT

Supporting Information

The Supporting Information is available free of charge on the ACS Publications website at DOI: 10.1021/acsomega.8b02890.

Optimized structure and relative energy of other possible isomers of NO adsorbed structure **2** and NO−CO and NO−NO coadsorbed structure **4**; potential energy curve for the N−O dissociative adsorption on Cu_{38}; geometry and energy change for NO dimerization on Cu_{38} and Cu_{55} calculated at the PBE functional with the plane wave basis sets; other possible reaction pathways of NO−CO reaction on Cu_{38}; natural orbitals of the NO dimer and the NO dimer on Cu_2 calculated by the CASSCF method; discussion about the electronic structure of the NO dimer by the CASSCF calculations; orbital energy change for NO dimerization and CO oxidation processes on Cu_{38}; XRD pattern of 5 wt % Cu/γ-Al_2O_3; geometrical parameters, NBO charges for CO oxidation processes on Cu_{38}; energy change for NO dimerization on Cu_{38} calculated at the PBE functional; basis set superposition error for NO and CO adsorption on Cu_{38}; spin multiplicity and the S^2 eigenvalues for the typical calculated species; NBO charges, and spin distribution of the NO dimer on Cu_2; complete ref 49 (PDF).

Cartesian coordinates and total energies of all the optimized structures in this work (XYZ).

■ AUTHOR INFORMATION

Corresponding Authors

*E-mail: ehara@ims.ac.jp (M.E.).

*E-mail: sakaki.shigeyoshi.47e@st.kyoto-u.ac.jp (S.S.).

ORCID

Hiroki Miura: 0000-0002-2488-4432

Tetsuya Shishido: 0000-0002-8475-4226

Ryoichi Fukuda: 0000-0003-3001-4190

Masahiro Ehara: 0000-0002-2185-0077

Shigeyoshi Sakaki: 0000-0002-1783-3282

Notes

The authors declare no competing financial interest.

■ ACKNOWLEDGMENTS

This work was carried out in "Element Strategy Initiative for Catalysts and Batteries (ESICB)", which is financially supported by the Ministry of Education, Culture, Science, Sports, and Technology (MEXT), Japan. S.S. wishes to thank the partial financial support from MEXT through JSPS KAKENHI (No. 15H03770) and the Ministry of Economy, Trade and Industry, Japan, through a project (P16010) commissioned by the New Energy and Industrial Technology Development Organization (NEDO). We wish to thank the computational center at the Institute of Molecular Science (Okazaki, Japan) for allowing the use of the computer and HPCI-Riken (Kobe, Japan) for the use supercomputer "K".

■ REFERENCES

(1) Cooper, J.; Beecham, J. A Study of Platinum Group Metals in Three-Way Autocatalysts. *Platinum Met. Rev.* **2013**, *57*, 281−288.

(2) Zhdanov, V. P.; Kasemo, B. Mechanism and kinetics of the NO-CO reaction on Rh. *Surf. Sci. Rep.* **1997**, *29*, 31−90.

(3) Dent, A. J.; Evans, J.; Fiddy, S. G.; Jyoti, B.; Newton, M. A.; Tromp, M. Rhodium Dispersion during NO/CO Conversions. *Angew. Chem., Int. Ed.* **2007**, *46*, 5356−5358.

(4) Olsson, L.; Zhdanov, V. P.; Kasemo, B. Role of steps in the NO−CO reaction on the (111) surface of noble metals. *Surf. Sci.* **2003**, *529*, 338−348.

(5) Rainer, D. R.; Koranne, M.; Vesecky, S. M.; Goodman, D. W. CO + O_2 and CO + NO Reactions over Pd/Al_2O_3 Catalysts. *J. Phys. Chem. B* **1997**, *101*, 10769−10774.

(6) Eichler, A.; Hafner, J. NO Reduction by CO on the Pt(100) Surface. A Density Functional Theory Study. *J. Catal.* **2001**, *204*, 118−128.

(7) Avalos, L. A.; Uñac, B. R.; Zaera, F.; et al. Dynamic Monte Carlo Simulation of the NO + CO Reaction on Rh(111). *J. Phys. Chem. B* **2006**, *110*, 24964−24971.

(8) Alas, S. J.; Vicente, L. Kinetic study of the "surface explosion" phenomenon in the NO+CO reaction on Pt(100) through dynamic Monte Carlo simulation. *J. Chem. Phys.* **2008**, *128*, 134705−134712.

DOI: 10.1021/acsomega.8b02890
ACS Omega 2019, 4, 2596−2609

(9) Xu, Q.-Q.; Yang, H.-Q.; Gao, C.; Hu, C.-W. Theoretical study on the reaction mechanism of NO and CO catalyzed by Rh atom. *Struct. Chem.* **2013**, *24*, 13−23.
(10) Haruta, M.; Kobayashi, T.; Sano, H.; Yamada, N. Novel Gold Catalysts for the Oxidation of Carbon Monoxide at a Temperature far Below 0 °C. *Chem. Lett.* **1987**, 405−408.
(11) Haruta, M.; Yamada, N.; Kobayashi, T.; Iijima, S. Gold catalysts prepared by coprecipitation for low-temperature oxidation of hydrogen and of carbon monoxide. *J. Catal.* **1989**, *115*, 301−309.
(12) Haruta, M. Chance and Necessity: My Encounter with Gold Catalysts. *Angew. Chem., Int. Ed.* **2014**, *53*, 52−56.
(13) Fajín, J. L. C.; Cordeiro, M. N. D. S.; Gomes, J. R. B. A DFT study of the NO dissociation on gold surfaces doped with transition metals. *J. Chem. Phys.* **2013**, *138*, 074701−074709.
(14) Beniya, A.; Ikuta, Y.; Isomura, N.; Hirata, H.; Watanabe, Y. Synergistic Promotion of NO-CO Reaction Cycle by Gold and Nickel Elucidated using a Well-Defined Model Bimetallic Catalyst Surface. *ACS Catal.* **2017**, *7*, 1369−1377.
(15) Shimizu, K.-I.; Shibata, J.; Yoshida, H.; Satsuma, A.; Hattori, T. Silver-alumina catalysts for selective reduction of NO by higher hydrocarbons: structure of active sites and reaction mechanism. *Appl. Catal., B* **2001**, *30*, 151−162.
(16) Meunier, F. C.; Breen, J. P.; Zuzaniuk, V.; Olsson, M.; Ross, J. R. H. Mechanistic Aspects of the Selective Reduction of NO by Propene over Alumina and Silver−Alumina Catalysts. *J. Catal.* **1999**, *187*, 493−505.
(17) Bogdanchikova, N.; Meunier, F. C.; Avalos-Borja, M.; Breen, J. P.; Pestryakov, A. On the nature of the silver phases of Ag/Al_2O_3 catalysts for reactions involving nitric oxide. *Appl. Catal., B* **2002**, *36*, 287−297.
(18) Bethke, K. A.; Kung, H. H. Supported Ag Catalysts for the Lean Reduction of NO with C_3H_6. *J. Catal.* **1997**, *172*, 93−102.
(19) Liu, Z.-P.; Jenkins, S. J.; King, D. A. Why Is Silver Catalytically Active for NO Reduction? A Unique Pathway via an Inverted $(NO)_2$ Dimer. *J. Am. Chem. Soc.* **2004**, *126*, 7336−7340.
(20) Mazheika, A. S.; Bredow, T.; Ivashkevich, O. A.; Matulis, V. E. Theoretical Study of NO Conversion on Ag/TiO_2 Systems. I. Anatase (100) Surface. *J. Phys. Chem. C* **2012**, *116*, 25262−25273.
(21) Mazheika, A. S.; Bredow, T.; Ivashkevich, O. A.; Matulis, V. E. Theoretical Study of NO Conversion on Ag/TiO_2 Systems. II. Rutile (110) Surface. *J. Phys. Chem. C* **2012**, *116*, 25274−25285.
(22) Shimizu, K.; Kawabata, H.; Maeshima, H.; Satsuma, A.; Hattori, T. Intermediates in the Selective Reduction of NO by Propene over $Cu\text{-}Al_2O_3$ Catalysts: Transient in-Situ FTIR Study. *J. Phys. Chem. B* **2000**, *104*, 2885−2893.
(23) Yamamoto, T.; Tanaka, T.; Kuma, R.; Suzuki, S.; Amano, F.; Shimooka, Y.; Kohno, Y.; Funabiki, T.; Yoshida, S. NO Reduction with CO in the Presence of O_2 over Al_2O_3-Supported and Cu-based Catalysts. *Phys. Chem. Chem. Phys.* **2002**, *4*, 2449−2458.
(24) Yen, M.-Y.; Ho, J.-J. Density-functional study for the NO_x (x = 1, 2) dissociation mechanism on the Cu(111) surface. *Chem. Phys.* **2010**, *373*, 300−306.
(25) Kacimi, M.; Ziyada, M.; Liotta, L. F. Cu on amorphous $AlPO_4$: Preparation, characterization and catalytic activity in NO reduction by CO in presence of oxygen. *Catal. Today* **2015**, *241*, 151−158.
(26) Sakai, M.; Nagai, Y.; Aoki, Y.; Takahashi, N. Investigation into the catalytic reduction of NO_x at copper−ceria interface active sites. *Appl. Catal., A* **2016**, *510*, 57−63.
(27) González, S.; Sousa, C.; Illas, F. Promoter and poisoning effects on NO-catalyzed dissociation on bimetallic RhCu(111) surfaces. *J. Catal.* **2006**, *239*, 431−440.
(28) Fukuda, R.; Takagi, N.; Sakaki, S.; Ehara, M. Structures of bimetallic copper-ruthenium nanoparticles: incoherent interface and surface active sites for catalytic nitric oxide dissociation. *J. Phys. Chem. C* **2017**, *121*, 300−307.
(29) Western, C. M.; Langridge-Smith, P. R. R.; Howard, B. J.; Novick, S. E. Molecular beam electric resonance spectroscopy of the nitric oxide dimer. *Mol. Phys.* **1981**, *44*, 145.
(30) McKellar, A. R. W.; Watson, J. K. G.; Howard, B. J. The NO dimer: ^{15}N isotopic infrared spectra, line widths and force field. *Mol. Phys.* **1995**, *86*, 273−286.
(31) Wade, E. A.; Cline, J. I.; K. Lorenz, T.; Hayden, C.; Chandler, D. W. Direct measurement of the binding energy of the NO dimer. *J. Chem. Phys.* **2002**, *116*, 4755−4757.
(32) Taniike, T.; Tada, M.; Coquet, R.; Morikawa, Y.; Sasaki, T.; Iwasawa, Y. A new aspect of heterogeneous catalysis: Highly reactive *cis*-$(NO)_2$ dimer and Eley−Rideal mechanism for NO−CO reaction on a Co-dimer/γ-alumina catalyst. *Chem. Phys. Lett.* **2007**, *443*, 66−70.
(33) Fajín, J. L. C.; Cordeiro, M. N. D. S.; Gomes, J. R. B. Unraveling the mechanism of the NO reduction by CO on gold based catalysts. *J. Catal.* **2012**, *289*, 11−20.
(34) Tsukuda, T.; Saeki, M.; Zhu, L.; Nagata, T. Formation of $N_3O_3^-$ anion in $(NO)_n^-$: photoelectron spectroscopy and ab initio calculations. *Chem. Phys. Lett.* **1998**, *295*, 416−422.
(35) Snis, A.; Panas, I. N_2O_2, $N_2O_2^-$ and $N_2O_2^{2-}$: structures, energetics and N-N bonding. *Chem. Phys.* **1997**, *221*, 1−10.
(36) Sayós, R.; Valero, R.; Anglada, J. M.; González, M. Theoretical investigation of the eight low-lying electronic states of the *cis*- and *trans*-nitric oxide dimers and its isomerization using multiconfigurational second-order perturbation theory (CASPT2). *J. Chem. Phys.* **2000**, *112*, 6608−6624.
(37) Tobita, M.; Perera, S. A.; Musial, M.; Bartlett, R. J.; Nooijen, M.; Lee, J. S. Critical comparison of single-reference and multi-reference coupled-cluster methods: Geometry, harmonic frequencies, and excitation energies of N_2O_2. *J. Chem. Phys.* **2003**, *119*, 10713−10723.
(38) Taguchi, N.; Mochizuki, Y.; Ishikawa, T.; Tanaka, K. Multi-reference calculations of nitric oxide dimer. *Chem. Phys. Lett.* **2008**, *451*, 31−36.
(39) Takagi, N.; Nakagaki, M.; Ishimura, K.; Fukuda, R.; Ehara, M.; Sakaki, S. Electronic Processes in NO Dimerization on Ag and Cu Clusters: DFT and MRMP2 Studies. *J. Comput. Chem.* **2019**, *40*, 181−190.
(40) Becke, A. D. Density-functional exchange-energy approximation with correct asymptotic behavior. *Phys. Rev. A* **1988**, *38*, 3098−3100.
(41) Becke, A. D. Density-functional thermochemistry. III. The role of exact exchange. *J. Chem. Phys.* **1993**, *98*, 5648−5652.
(42) Lee, C.; Yang, W.; Parr, R. G. Development of the Colle-Salvetti correlation-energy formula into a functional of the electron density. *Phys. Rev. B* **1988**, *37*, 785−789.
(43) Stroppa, A.; G Kresse, G. The shortcomings of semi-local and hybrid functionals: what we can learn from surface science studies. *New J. Phys.* **2008**, *10*, No. 063020.
(44) Takagi, N.; Ishimura, K.; Matsui, M.; Fukuda, R.; Ehara, M.; Sakaki, S. Core-Shell versus Other Structures in Binary $Cu_{38-n}M_n$ Nanoclusters (M = Ru, Rh, Pd, Ag, Os, Ir, Pt, and Au; n = 1, 2, and 6): Theoretical Insight into Determining Factors. *J. Phys. Chem. C* **2017**, *121*, 10514−10528.
(45) Hay, P.; Wadt, W. R. Ab initio effective core potentials for molecular calculations. Potentials for K to Au including the outermost core orbitals. *J. Chem. Phys.* **1985**, *82*, 299−310.
(46) Dunning, T. H., Jr.; Hay, P. J. In *Modern Theoretical Chemistry*; Schaefer, H. F., III, Ed.; Plenum: New York, 1976; Vol. 3, pp 1−28.
(47) Roos, B. O. The Complete Active Space Self-Consistent Field Method and its Applications in Electronic Structure Calculations. *Adv. Chem. Phys.* **1987**, *69*, 399−445.
(48) Dunning, T. H., Jr. Gaussian basis sets for use in correlated molecular calculations. I. The atoms boron through neon and hydrogen. *J. Chem. Phys.* **1989**, *90*, 1007−1023.
(49) Frisch, M. J.;et al. *Gaussian 09*, revision D.01; Gaussian, Inc.: Wallingford, CT, 2013.
(50) Ishimura, K. SMASH-1.1.0. http://smash-qc.sourceforge.net/ (accessed Jan, 2013).
(51) Schmidt, M. W.; Baldridge, K. K.; Boatz, J. A.; Elbert, S. T.; Gordon, M. S.; Jensen, J. H.; Koseki, S.; Matsunaga, N.; Nguyen, K.

DOI: 10.1021/acsomega.8b02890
ACS Omega 2019, 4, 2596−2609

A.; Su, S.; Windus, T. L.; Dupuis, M.; Montgomery, J. A. General Atomic and Molecular Electronic Structure System. *J. Comput. Chem.* **1993**, *14*, 1347−1363.
(52) Itoh, M.; Kumar, V.; Adschiri, T.; Kawazoe, Y. Comprehensive study of sodium, copper, and silver clusters over a wide range of sizes $2 \leq N \leq 75$. *J. Chem. Phys.* **2009**, *131*, 174510−174528.
(53) Johnson, D. W.; Matloob, M. H.; Roberts, M. W. Adsorption of nitric oxide on Cu(100) surfaces; an electron spectroscopic study. *J. Chem. Soc. Chem. Commun.* **1978**, 40−41.
(54) Matloob, M. H.; Roberts, M. W. Electron spectroscopic study of nitrogen species adsorbed on copper. *J. Chem. Soc., Faraday Trans. 1* **1977**, *73*, 1393−1405.
(55) Johnson, D. W.; Matloob, M. H.; Roberts, M. W. Study of the interaction of nitric oxide with Cu(100) and Cu(111) surfaces using low energy electron diffraction and electron spectroscopy. *J. Chem. Soc., Faraday Trans. 1* **1979**, *75*, 2143−2159.
(56) Dhesi, S. S.; Haq, S.; Barrett, S. D.; Liebsle, F. M. LEED and STM studies of structures formed by NO dissociation on Cu(100) surfaces. *Surf. Sci.* **1996**, *365*, 602−613.
(57) Wee, A. T. S.; Lin, J.; Huan, A. C. H.; Loh, F. C.; Tan, K. L. SIMS study of NO, CO adsorption on Cu(100) and Cu(210) surfaces. *Surf. Sci.* **1994**, *304*, 145−158.
(58) Matulis, V. E.; Palagin, D. M.; Mazheika, A. S.; Ivashkevich, O. A. Theoretical study of NO adsorption on neutral, anionic and cationic Ag_8 clusters. *Comput. Theor. Chem.* **2011**, *963*, 422−426.

DOI: 10.1021/acsomega.8b02890
ACS Omega 2019, 4, 2596−2609